Astron. Astrophys. 294, 241–251 (1995)

ASTRONOMY AND ASTROPHYSICS

Acoustic wave propagation in the solar atmosphere

II. Nonlinear response to adiabatic wave excitation

G. Sutmann and P. Ulmschneider

Institut für Theoretische Astrophysik der Universität Heidelberg, Im Neuenheimer Feld 561, D-69120 Heidelberg, Germany

Received 31 March 1994 / Accepted 21 May 1994

Abstract. We study the response of the solar atmosphere to excitations with adiabatic large amplitude acoustic waves. Both monochromatic waves and acoustic spectra are considered. For monochromatic excitation a critical frequency ν_{cr} is found which separates different domains of resonance behaviour. Upon excitation with frequencies $\nu < \nu_{cr}$ the atmospheric resonance decays rapidly with time as in the small amplitude wave case, while for $\nu > \nu_{cr}$, persistent resonance oscillations occur which are caused by shock overtakings. Excitation by acoustic spectra always leads to the $\nu > \nu_{cr}$ behaviour. Independent of the spectral shape and energy, acoustic spectra generate oscillations mainly at frequencies $\nu = 6 - 7$ mHz at the top of the chromosphere. The photospheric 5-min oscillation does not influence our chromospheric results. Shock heating by acoustic spectra is roughly similar to that of a monochromatic wave of period 35 s. Irrespective of the initial spectral shape and energy and even of the gravity and effective temperature of the star, a universal average shock strength $M_S = 1.5$ is found. Due to our adiabatic treatment, the atmospheric slabs suffer extension which grows with wave energy.

Key words: hydrodynamics – shock waves – waves – Sun: chromosphere – Sun: oscillations

1. Introduction

The pronounced signal of velocity and temperature fluctuations in the solar chromosphere, seen in the Ca II H and K, Hα and the Ca II infrared triplet lines, is one near 3 min (ν = 5.5mHz). For recent detailed reviews of the 3 min oscillations see Deubner (1991), Fleck & Schmitz (1991) as well as Rutten & Uitenbroek (1991). Fleck & Schmitz (1991) were the first to show that the 3-min oscillation, instead of being a cavity mode, is explained simply as the basic cut-off frequency resonance of the chromosphere. This view has been confirmed by Kalkofen et al. (1994) as well as by us (Sutmann & Ulmschneider 1994, henceforth called Paper I). The atmospheric resonance is due to a local oscillation of gas elements around their rest position in hydrostatic equilibrium, while cavity modes depend on the detailed geometrical extent of the cavity.

However, it has been recognized (Rammacher & Ulmschneider 1992; Fleck & Schmitz 1993; Kalkofen et al. 1994) that this resonance behaviour, which can readily be deduced both analytically and numerically in the case of small amplitude perturbations of the atmosphere, is not yet fully understood in cases where the perturbation amplitudes are not small. In such cases shocks occur which, by the process of shock overtaking, can greatly modify the atmospheric response.

In this second paper we intend to complement and extend the work of Fleck & Schmitz (1993) as well as Kalkofen et al. (1994) and study in greater detail the response of the solar atmosphere to large amplitude acoustic wave perturbations. In particular we investigate the response of the atmosphere to the excitation by monochromatic short period waves as well as by several types of wave spectra, where most frequencies lie above the cut-off frequency. We also discuss cases with a superposed photospheric 5 min oscillation and study the mechanical energy dissipation behaviour. In Sect. 2 we outline our numerical methods. Section 3 presents the results while Sect. 4 gives our conclusions.

2. Method

2.1. Wave calculations and Fourier analysis

The method of wave computation has been described in Paper I and we refer to that paper for further details. The time–dependent hydrodynamic equations are solved for an atmospheric slab using the method of characteristics. We follow the development of the originally linear wave (introduced at the bottom of the atmosphere by a piston) to the point of shock formation and beyond. The shocks are treated as discontinuities and are allowed to grow to arbitrary strength. They are also permitted to overtake one another. The main difference to Paper I is that we now assume larger, realistic acoustic wave fluxes in the range $F_M = 1 \cdot 10^6$ to $1 \cdot 10^9$ erg cm^{-2}s^{-1} which lead to shocks. However, similar to Paper I, we neglect radiation effects and assume adiabatic conditions.

The use of Fourier analysis and the evaluation of velocity power spectra is the same as described in Paper I and we refer the reader to that paper for details. The only difference compared to Paper I is that we now frequently have to interpolate at points close to shock discontinuities in order to obtain an equidistant time- and height grid. Regions away from the shocks are interpolated with the method of weighted parabolas as in Paper I, while regions close to shocks are interpolated linearly.

2.2. Atmosphere models

As it was shown for the linear case in Paper I the resonance behaviour of the solar atmosphere depends on the type of the atmosphere model. To study the nonlinear behaviour we have selected four types of models shown in Fig. 1. We take a pure H^- radiative equilibrium model, a combined H^- and Mg II k radiative equilibrium model, model C of Vernazza et al. (1981) and an isothermal model with $T = 5000\ K$. The radiative equilibrium models have been constructed using temperature correction procedures discussed by Cuntz et al. (1994).

2.3. Wave spectra

At the bottom boundary, velocity fluctuations are prescribed by using a piston. Similarly to the cases discussed in Paper I we have selected four types of frequency spectra with $N+1 = 101$ partial waves each. The frequencies $\omega_n = 2\pi\nu_n$ of the partial waves are usually chosen such that one has equidistant intervals $\nu_{i+1} - \nu_i =$ 0.5 mHz around a central frequency $\omega_{N/2} = 2\pi/35\ Hz$. The piston velocity is prescribed by the superposition

$$u(t) = c \sum_{n=0}^{N} M_n \ \sin(\omega_n t + \varphi_n) \quad , \tag{1}$$

where the M_n are Mach numbers of the partial waves and the φ_n arbitrary but constant phase angles. As the velocity amplitude at the piston is small, the mechanical energy flux F_M can be written using linear theory

$$\begin{aligned} F_M &= \frac{1}{T}\int_0^T p' u dt \\ &= \frac{1}{T}\int_0^T \rho c^3 \sum_{n=0}^{N} (M_n \sin(\omega_n t + \varphi_n))^2 \ \cos\alpha_n dt \end{aligned} \quad , \tag{2}$$

where T is an arbitrary but sufficiently long time for the time averaging, p' the complex pressure perturbation, u the complex velocity amplitude, ρ the density and α_n the phase shift between velocity- and pressure fluctuations given by

$$\alpha_n = \arctan\left(\frac{\omega_A}{\sqrt{\omega_n^2 - \omega_A^2}}\right) \quad , \tag{3}$$

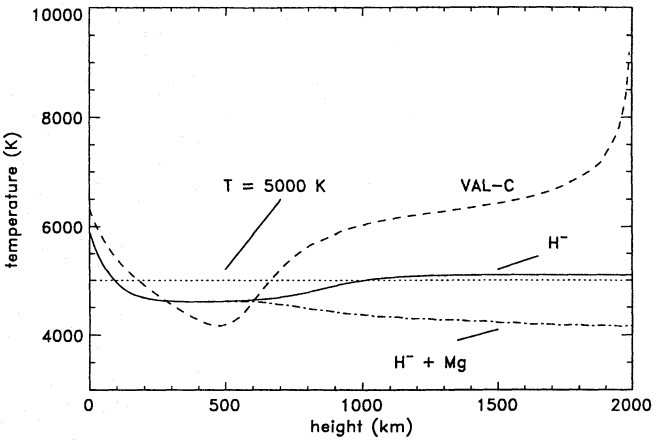

Fig. 1. Temperature distribution of various solar atmosphere models used in this paper

where $\omega_A = \gamma g/(2c)$ is the acoustic cut-off frequency at the bottom of the atmosphere. As we want to study the behaviour of different velocity spectra under similar initial conditions, we normalize the velocity amplitudes to a given acoustic energy flux. So we take for the Mach numbers of the partial waves

$$M_n = q\sqrt{\frac{F_M}{\rho c^3}}\ f(\omega_n) \quad , \tag{4}$$

where q is a normalization factor and $f(\omega_n)$ a spectral distribution function of the partial waves described below. The normalization factor q is chosen such that upon introduction of Eqs. (3) and (4) into (2), the prescribed flux F_M is obtained. The mechanical energy flux was chosen in the range $F_M = 1 \cdot 10^6$ to $1 \cdot 10^9$ ergcm^{-2}s^{-1}.

For the four different spectra we choose four different distribution functions $f(\omega_n)$.

a) Box spectrum: all partial waves have a constant amplitude given by the Mach number M_{00}. We take

$$f(\omega_n) = \mathcal{N}_B M_{00} \quad , \tag{5}$$

over the prescribed frequency interval $\Delta\omega = \omega_N - \omega_0$. Here and in the following cases the quantities $\mathcal{N}$ denote normalization factors which arise from the fact that we want $f(\omega_n)$ to be normalized to one.

b) Gauss spectrum: the partial waves are distributed in a Gauss distribution around a central frequency ω_C. We use

$$f(\omega_n) = \mathcal{N}_G \exp\left\{-\frac{(\omega_n - \omega_C)^2}{2\omega_\sigma^2}\right\} \quad , \tag{6}$$

where usually $\omega_C = \omega_{N/2} = 2\pi/35\ Hz$ was chosen. The width of the Gaussian distribution was chosen as $\omega_\sigma = 2\omega_A$.

c) Random spectrum: the partial waves have randomly chosen amplitudes, here we have

$$f(\omega_n) = \mathcal{N}_R Z(\omega_n) M_{00} \quad , \tag{7}$$

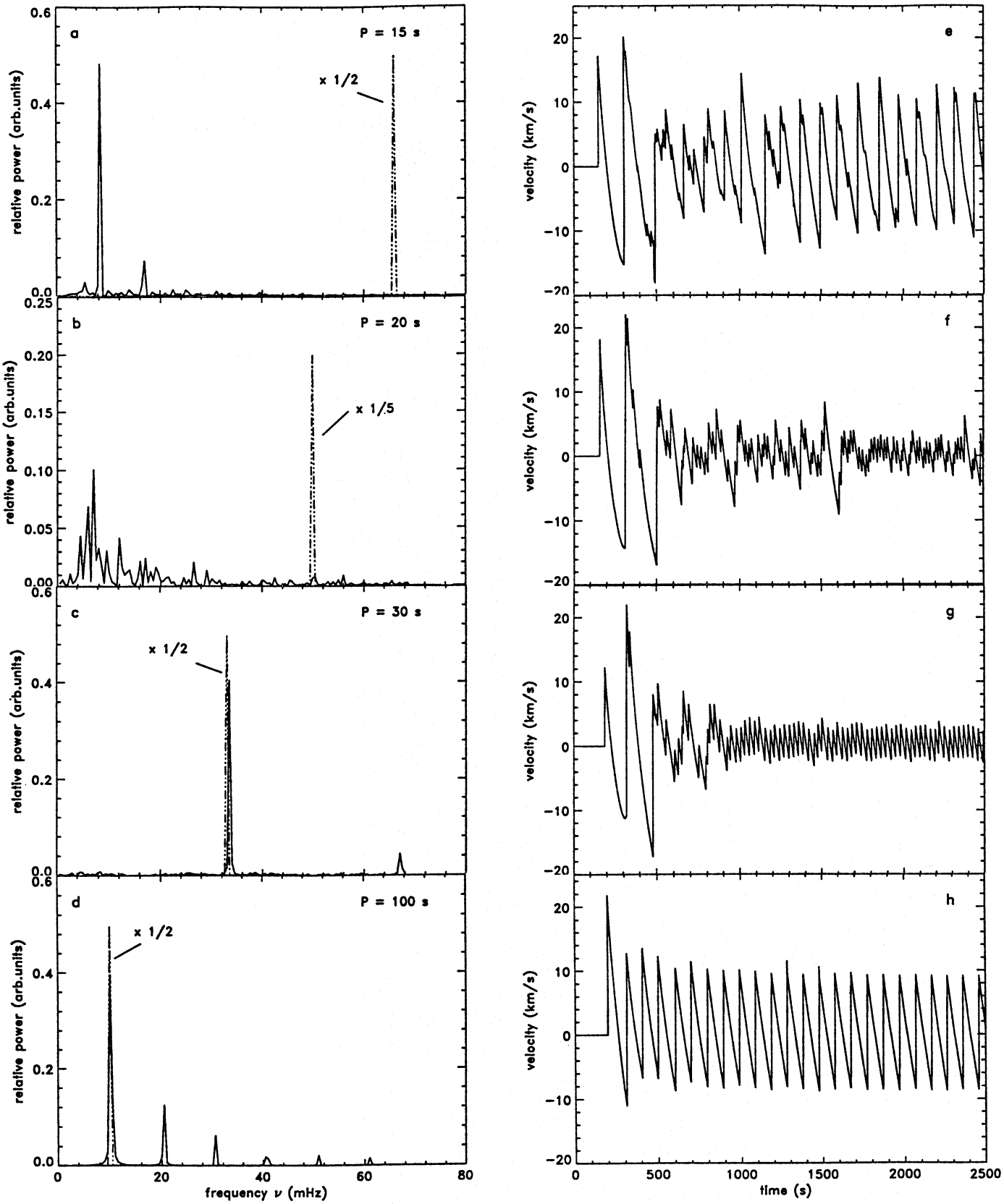

Fig. 2. Power spectra (left panels) and velocities at height z_{top} = 2000 km (right panels) for an excitation with monochromatic waves of different indicated periods. The power spectra are shown at the bottom of the atmosphere at height z = 0 km (dashed) and at height z_{top} (drawn)

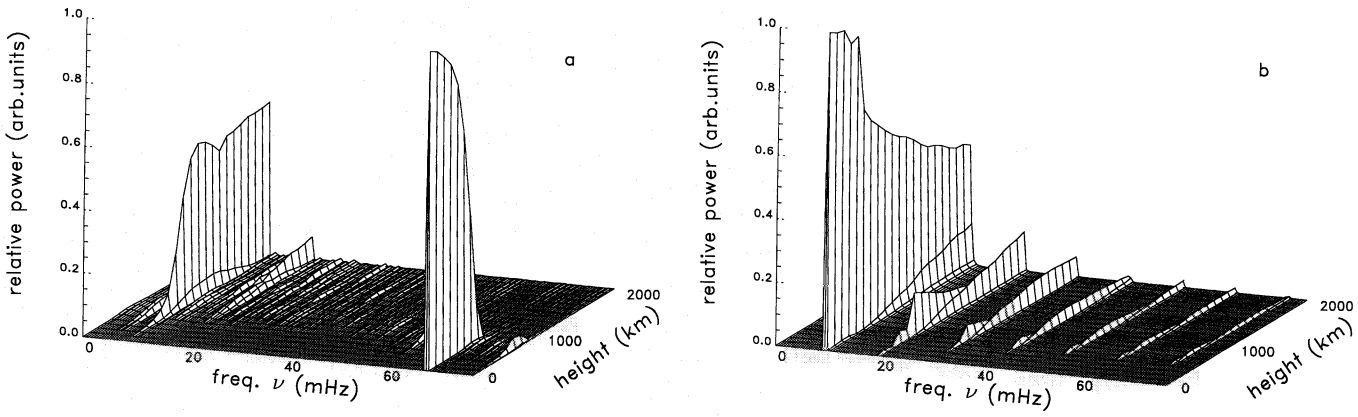

Fig. 3a and b. Power spectra as functions of frequency and height for the excitation with monochromatic waves **a** with period P = 15 s and **b** with P = 100 s

where $Z(\omega_n)$ is a random number in the interval [0,1] and M_{00} a constant Mach number.

d) Exponential spectrum: the partial wave amplitudes decrease exponentially with frequency. We take

$$f(\omega_n) = \mathcal{N}_E \exp\left\{-\frac{\omega_n}{\omega_\sigma}\right\} \quad , \tag{8}$$

where $\omega_\sigma = 4\,\omega_A$ was chosen. The four different types of incident acoustic wave spectra are shown in Fig. 4.

3. Results

3.1. Excitation by monochromatic waves

On the basis of a pure H^- model we first studied the monochromatic waves taking a realistic acoustic flux of $F_M = 1 \cdot 10^8$ erg cm^{-2}s^{-1}. Figure 2 show the power spectra both at the bottom $z = 0\ km$ (dashed) and at Euler height $z = 2000\ km$ (drawn) for waves of period P = 15, 20, 30, 100 s. In addition, for the four waves, the velocities at height $z = 2000\ km$ are shown as a function of time. The Euler height $z = 2000\ km$ is henceforth called z_{top}, although our top Lagrange point, due to the adiabatic nature of our wave calculation, expands to considerably larger Euler heights.

The right panels of Fig. 2 show that at $z = z_{top}$ all waves have been transformed into sawtooth shock waves and that after about 500 s, that is, in less than 3 cut-off periods, the initial transient resonance has essentially died out. This resonance results from the start of the calculation, where the wave propagates into the undisturbed atmosphere. The rapid decay of the resonance is in good agreement with the linear results of Paper I for positive temperature gradient atmospheres. The left panels of Fig. 2 show both a similar and a distinctly different behaviour compared to the linear wave calculations in Paper I. The waves of P = 30 and 100 s (Fig. 2c, 2d, 2g, 2h) both show what we would expect from Paper I. After the decay of the resonance only the exciting wave survives, together here with overtone components, which are the Fourier components of the sawtooth wave.

The P = 15 s and, to a lesser degree, the 20 s waves show a very different behaviour. Figure 2a, 2e and particularly Fig. 3a show that the P = 15 s wave is almost completely obliterated at and even much below the height z_{top} in favour of a resonance oscillation at about 8 mHz (125 s) with amplitudes of roughly 2/3 the initial transient resonance of the atmosphere. Although the P = 20 s wave still shows some of its original wave period at z_{top}, the power spectrum indicates that most of the power is in the low frequencies with a peak near 6 mHz.

There appears to be a *critical frequency* ν_{cr} near 40 mHz (25 s) which separates two domains of radically different resonance behaviour. For incident waves with frequency $\nu < \nu_{cr}$ the resonance behaviour of the atmosphere is essentially that of a linear wave excitation. An initial resonance develops, caused by the switch-on process from starting the calculation. After the rapid decay of this resonance only the incident wave survives. For excitation with frequency $\nu > \nu_{cr}$, however, a persistent resonance behaviour is found. This resonance behaviour is generated by shock overtakings which act as repeated switch-on processes.

As in a shock overtaking event a following shock catches up and merges with a more slowly moving leading shock, it is clear that this event depends sensitively on the spatial distance between the two shocks, that is, on the wavelength. Thus shock overtakings occur more easily for short period waves which explains the existence of a critical wave period. The differences in shock propagation speed (which causes the shock overtakings) result from the spatial temperature variations associated with the resonance oscillations of the atmosphere. The strong shocks created from the overtaking events rekindle the atmospheric resonance which otherwise would decay.

That shock overtakings can cause long period atmospheric resonance oscillations and that there is a critical wave period below which this occurs has also been found by Rammacher & Ulmschneider (1992). In their calculations, different from our present computations because radiation damping was included, they find a critical wave period slightly larger than P = 30 s. It has been proposed that this process of conversion of short period wave energy into long period fluctuations could be important for driving mass loss in red giants (Ulmschneider et al. 1992).

Figure 3 show the height dependence of the radically different resonance behaviour in the domains above and below ν_{cr}.

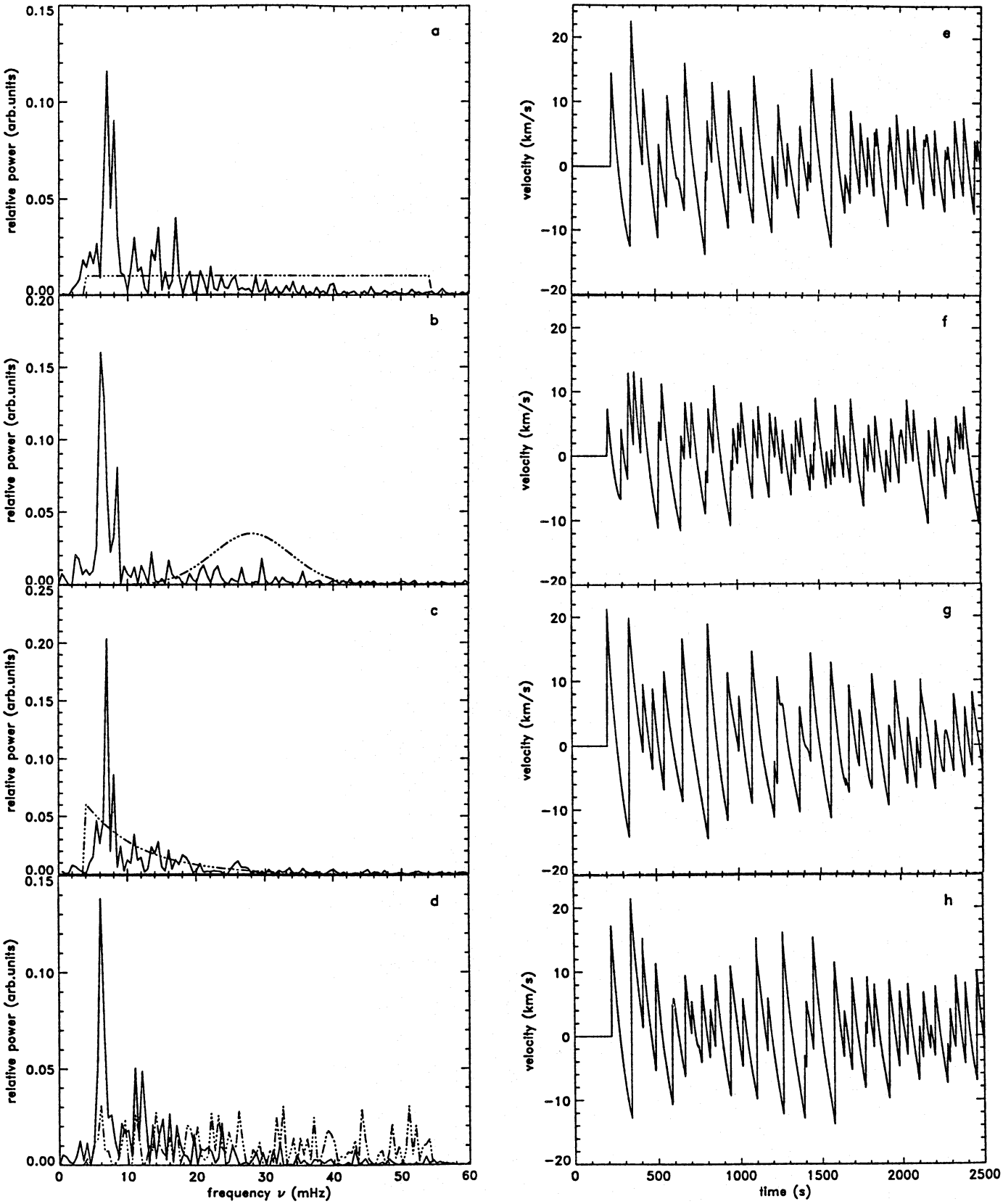

Fig. 4a–h. Power spectra (left panels) and velocities (right panels) for an excitation with four different incident acoustic frequency spectra **a** box spectrum, **b** Gauss spectrum with maximum at P = 35 s, **c** exponential spectrum, **d** random spectrum. The power spectra are shown at height $z = 0\ km$ (dashed) and $z_{top} = 2000\ km$ (drawn), the velocities (according to **e** box spectrum, **f** Gauss spectrum, **g** exponential spectrum, **h** random spectrum) at height z_{top}

In Fig. 3a it is seen that the high frequency incident wave in the layers below $z = 1000\ km$ gets destroyed by overtaking shocks (for a time sequence of such an overtaking event see Fig. 7 of Rammacher & Ulmschneider 1992). Figure 3b shows that the low frequency wave survives the transit through the atmosphere and that there is a height dependent growth of the overtone spectrum.

Our results on the excitation by monochromatic waves are in good agreement with those of Kalkofen et al. (1994, their Fig. 9), who took a much wider atmospheric slab. Their wave with $P = 37$ s shows the $\nu < \nu_{cr}$ behaviour below 15 scale heights in agreement with us, but at greater heights in their initially isothermal atmosphere these waves due to shock overtaking get completely destroyed, with only the resonance oscillation surviving. This shows that the critical frequency ν_{cr}, in principle, is a function of height, because in a wider atmospheric slab, longer period waves will be able to overtake. However, the choice of the atmospheric slab is not arbitrary as will be discussed below in Sect. 3.6.

As it has been suggested that interaction with the non- propagating photospheric 5 min oscillation may feed energy into the chromospheric oscillation we test if the inclusion of the 5 min oscillation changes the above results. We superpose over the piston motion an additional velocity excitation with amplitude $u_5 = 1.5 \cdot 10^5$ cm/s and period $P = 300$ s. We find that the behaviour at z_{top} does not change compared to the case without the 5 min excitation. The same critical frequency with complete separation of the response regimes was found. In none of the cases did the 5 min oscillation survive to the top of the atmosphere. This is in agreement to our linear results of Paper I, were we found that compared to the propagating part of the spectrum essentially nothing survives of the evanescent part.

An interesting case which we have not computed is that of a continuous monochromatic excitation by a 5 min oscillation shown by Kalkofen et al. (1994). As we expect, it is seen that in this case the incident evanescent wave is severely damped but that the strong harmonics which are in the propagating region of the spectrum show the typical behaviour of these waves already discussed.

3.2. *Excitation with acoustic frequency spectra*

For an excitation with an acoustic frequency spectrum there is no defined wave period or wave amplitude in timespans small compared to times $\Delta t = 1/\Delta\nu$, where $\Delta\nu$ is the frequency interval of the equidistant frequency grid. As the formation of shocks depends on both the wave period and the amplitude, one does not have a well defined shock formation height. In addition, as shocks of different strength have different speeds, a spectrum more easily leads to shock overtakings. As discussed above, we investigated four different spectra with 101 frequency points each, spaced by $\Delta\nu = 0.5$ mHz. The lowest frequency point was about a factor of 0.7 below a cut-off frequency $\nu_A \approx 5$ mHz, while the highest frequency was about a factor of 11 greater.

The left panels of Fig. 4 show the power spectra of the velocity oscillations at the bottom $z = 0$ (dashed) and at the Euler

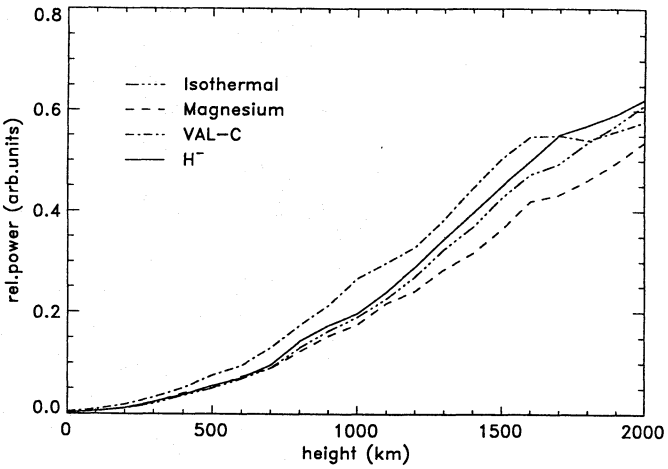

Fig. 5. Relative power in the band < 10 mHz as a function of height for the Gauss spectrum and four indicated initial atmosphere models

height z_{top} (drawn) for our four input spectra, together with the velocities (right panels) at height z_{top}. Despite the very different input at the bottom it is seen that the power spectra at $z = z_{top}$ differ very little. In all four spectra a dominant peak at $\nu = 6 - 7$ mHz is seen at that height. There is the tendency in all spectra that the low frequency resonant contributions dominate. This is due to the fact that the shock overtakings, that is, the stochastic nature of the spectra prevails. It is seen from the right panels of Fig. 4 that the shock overtakings have primarily consumed the short period wave components such that little high frequency wave power survives at height z_{top}.

The dominance of the resonance frequency component is clearly not the result of an initially large low frequency wave contribution. This is seen in the power spectrum of the exponential spectrum (Fig. 4c), where an initial maximum at 4 mHz is shifted to 7 mHz at z_{top}. The reason for the similarity of the four spectra is simply the stochastic resonances produced by the process of shock overtaking.

The general behaviour found for our spectra displayed in Fig. 4 agrees well with that found by Kalkofen et al. (1994). It also agrees with that found by Fleck & Schmitz (1993) who consider similar acoustic spectra, although they found somewhat larger resonance frequencies and a much broader spectrum. We attribute these differences to the low energy flux they took (see discussion to our Fig. 7 below). In addition we notice a persistent systematic height-independent flow in all of their velocities which we do not find in our work or that of Kalkofen et al. (1994). As from the expansion of the topmost mass point we would expect a flow which increases with height (see Sect. 3.6 below) in the Euler frame, we suspect that this systematic flow may be caused by their boundary conditions.

Same as in the case of monochromatic waves we have superposed an additional 5 min oscillation over our four wave spectra. To compare the results we, took the same mechanical energy fluxes as in the case without superposition. For a Gauss spectrum the resulting power spectrum at height z_{top}, is displayed in Fig. 6a. It is seen that there is essentially no change compared

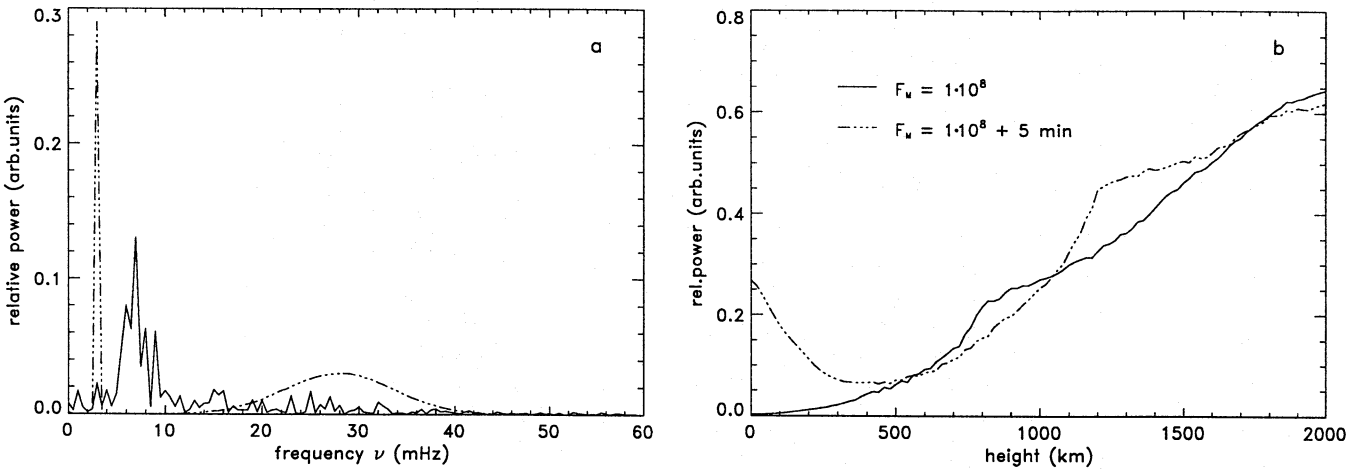

Fig. 6. a Power spectra for an excitation with a Gauss spectrum similar to Fig. 4b but for an additional excitation with a 5 min oscillation. **b** Relative power in the band < 10 mHz as a function of height for the same wave computations with (dashed) and without an additional 5 min oscillation (drawn)

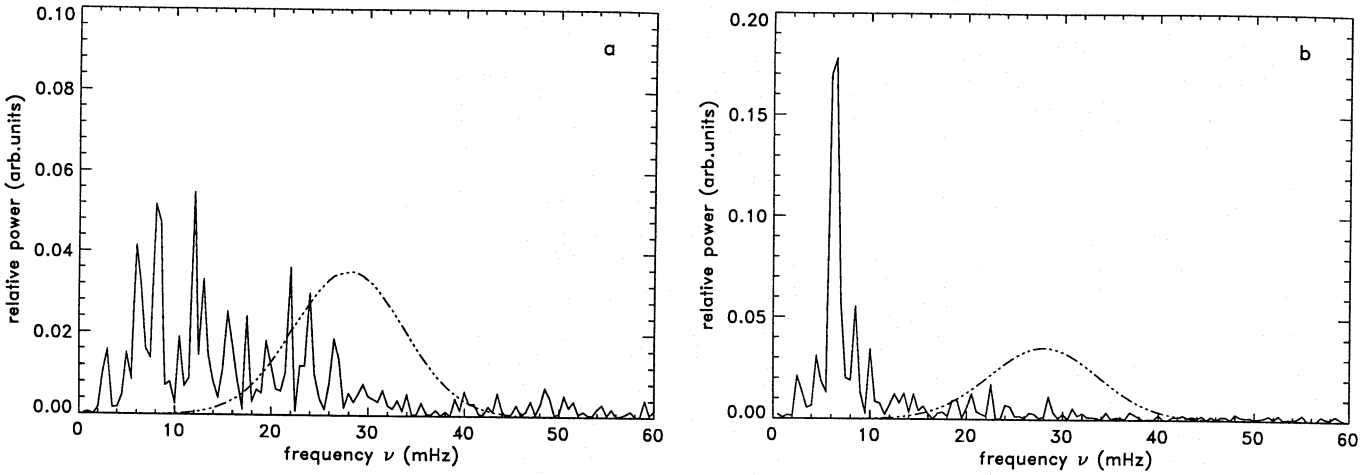

Fig. 7a and b. Power spectra for an excitation with a Gauss spectrum similar to Fig. 4b but for an incident flux **a** of $F_M = 1 \cdot 10^6$ and **b** $F_M = 1 \cdot 10^9$ erg cm^{-2}s^{-1}

to the power spectrum (Fig. 4b) without the 5 min oscillation. The same result was found for the superposition of the 5 min oscillation over the other three acoustic spectra. This contradicts results from Fleck & Schmitz (1993) who found that the 5 min oscillations strongly modified the low frequency spectrum: "It is only here in case 4 with the additional 5 min component ... where we see 3-min oscillations in the chromosphere". Even a switch-on effect by the onset of a strong 5 min oscillation will not affect the low frequency spectrum much because of the rapid decay of the resonance as already noted in Fig. 2 and as also seen in Fig. 4. The much more frequent shock overtakings of the acoustic spectrum dominate the low frequency behaviour.

The reason for the negligible influence of the 5 min oscillation for both the acoustic spectra and the monochromatic waves as discussed above is that these waves are non-propagating and thus are damped as a function of height (see Paper I). This damping effect with height is readily seen in Fig. 6b which displays the fraction of the power below 10 mHz as a function of height for the wave calculations both with and without an additional 5 min oscillation. At z_{top} the power below 10 mHz is roughly 60%.

Changing the shape of the spectra, e.g. the position of the maximum P_{max} of the Gauss spectrum did not alter much the resulting power spectrum from that found in Fig. 4, nor was the power spectrum influenced much by the number of frequency points. The power spectra at z_{top} moreover were similar to those produced by excitation with monochromatic waves of frequency greater than the critical frequency ν_{cr}.

3.3. Dependence on the atmosphere model

We have checked whether the power spectra at $z = z_{top}$ depended on the atmosphere models used. Calculations with the radiative equilibrium model H^- + Mg II k, the VAL-C model and the isothermal model with $T = 5000\ K$ did not change much the power spectra at z_{top}. This is seen in Fig. 5 which

displays the relative power below 10 mHz for all four models. This in agreement with Fleck & Schmitz (1993) we attribute to the fact that our strongly nonlinear waves destroy the initial atmospheric structure.

3.4. Dependence on the mechanical energy flux

We now discuss how the total incident mechanical flux affects the response of the atmosphere. We have studied the Gauss spectrum with P_{max} = 35 s, taking total integrated incident fluxes of $F_M = 1 \cdot 10^6$, $1 \cdot 10^7$, $1 \cdot 10^8$, $1 \cdot 10^9$erg cm^{-2}s^{-1}. As shown in Fig. 7 we found that the power spectra at height z_{top}, regardless of the initial flux F_M, peak at $6 - 7$ mHz, and are very similar to those of Fig. 4, except for the spectrum with the lowest flux, which is considerably broader in the low frequency band. In addition we found that with larger F_M the width of the resonance peak of the power spectra is narrower, the relative fraction of power $<$ 10 mHz is larger, the shock formation occurs earlier, the number of shock overtakings is greater and the heights where overtakings start to occur is lower. All these properties can be attributed to the fact that for a more energetic wave the steepening and the shock formation occurs earlier. For higher F_M the process of shock overtaking occurs at lower heights and the created strong shocks more quickly obliterate the high frequency components.

This interpretation is supported by Fig. 8 which displays the relative fraction of power $<$ 10 mHz as a function of height for the four energy fluxes F_M. Figure 8 shows that for greater initial flux more energy is converted into the low frequency band. This process is also seen in Fig. 9a where the maximum shock strength M_S is plotted which occurs at a given height. Figure 9a shows that the shock strengths due to shock overtaking increase with height in a rather discontinuous manner. It is also seen that with increasing F_M strong shocks occur at progressively lower heights.

3.5. A universal average shock strength

At this point we want to discuss a fairly surprising result. For a given height z consider a height range $z \pm \Delta z$ with say Δz = 100 km. In this height range we monitor all shocks, add up the shock strengths, and divide by the number of shocks. This crudely gives an *average shock strength* M_S per shock. As seen in Fig. 9b this average shock strength has a roughly constant value $M_S \approx 1.5$ for all four wave calculations with different initial flux F_M. Figure 9c shows the corresponding shock strengths M_S for monochromatic wave calculations using the same four initial energy fluxes and a period of P = 35 s. The shock strengths of Fig. 9b and 9c agree because of our choice of the monochromatic wave period. Due to the limiting strength behaviour of monochromatic waves (Ulmschneider 1991) the shock strength is proportional to the wave period and thus can be chosen by selecting the right period.

Independent of the initial energy flux, of the type of the initial spectrum and largely independent of the solar atmosphere model we find that the acoustic spectra produce average shock

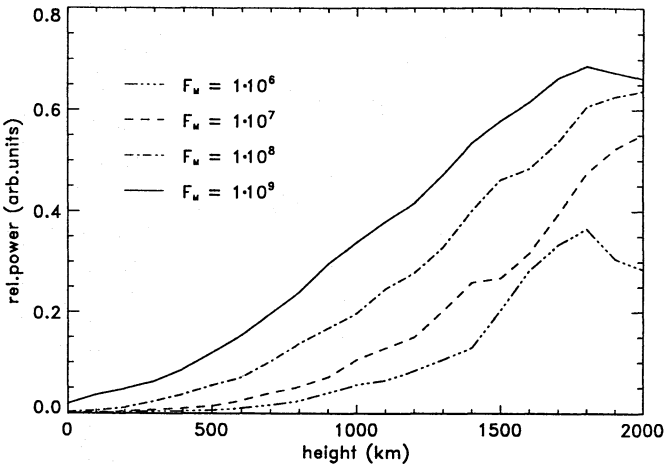

Fig. 8. Relative power in the band $<$ 10 mHz as a function of height for the Gauss spectrum and four indicated initial energy fluxes F_M

strengths which correspond crudely to monochromatic waves of period P = 35 s for the Sun. A similar universal strength of shock waves has been postulated by Ulmschneider (1990) on basis of acoustic energy spectra calculated from stellar convection zones and from limiting shock strength arguments. It was found that this universal shock strength applied to all late-type stars, irrespective of the effective temperature T_{eff} and gravity g. This tempted us to investigate whether the same average shock strength would also appear in acoustic wave spectrum calculations for stars other than the Sun.

We thus performed a similar acoustic wave calculation for a red giant star with T_{eff} = 5012 K and $\log g$ = 3 described by Cuntz et al. (1994). Here the acoustic spectrum had to be scaled according to the much lower acoustic cut-off frequency $\nu = \omega/(2\pi) \approx 1 \cdot 10^{-4}$ Hz of the giant, to ensure that one is in the propagating acoustic wave band, generated in the giant's convection zone (see Musielak et al. 1994; Cuntz et al. 1994). We were quite surprised to find (see Fig. 9d) that indeed the same average shock strength of M_S = 1.5 was found as in the case of the Sun, which means that this shock strength may be a universal quantity. Because the physical significance of this result and its possible similarity to the limiting shock strength results is not easily elucidated, we reserve a detailed discussion of this effect for a later investigation.

3.6. The expansion of the atmosphere

We now discuss a considerable shortcoming of the present investigation. We have seen that computations with realistic acoustic energy fluxes invariably lead to shocks and shock overtaking. Shock overtaking, where two shocks combine to form a single stronger shock, affects not only the heating but also the momentum deposition onto the gas. It thus is not surprising that our calculations show extensive expansions of the upper parts of our atmosphere models. This in our case is almost exclusively due to the neglect of radiation, that is, to our adiabatic approximation. The dissipated shock energy instead of going primarily

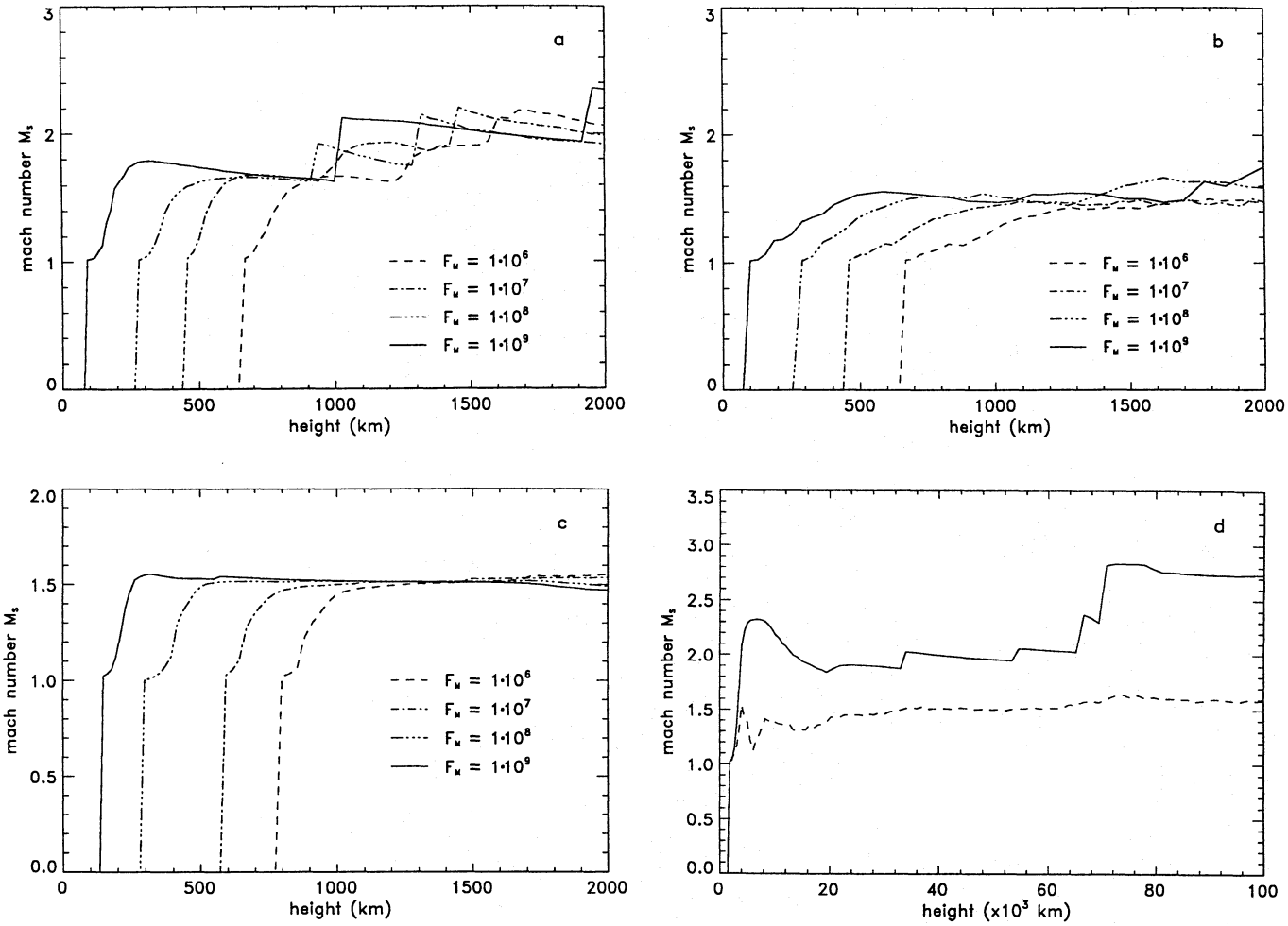

Fig. 9. a Maximum shock strength M_S as a function of height for the Gauss spectrum and different initial energy fluxes F_M. **b** Average shock strength M_S of the Gauss spectra. **c** Shock strength M_S as a function of height for monochromatic acoustic waves of different initial energy fluxes F_M. **d** Maximum (drawn) and average shock strength M_S (dashed) of acoustic waves in the atmosphere of a red giant of T_{eff} = 5012 K and log g = 3, excited by a Gauss spectrum

into radiation, in our case almost exclusively goes into the expansion of the medium.

Figure 10 shows the time development of the Euler heights of 12 mass elements (Lagrange points) spaced at equal height distances over our initial atmosphere model. This model has a minimum of 110 height points plus two infinitesimally close height points for each of the roughly 20 shocks present. In the course of the calculation the topmost Lagrange point in the calculation (with an initial flux $F_M = 10^8$ erg cm$^{-2}s^{-1}$) has moved (during the timespan Δt = 3000 s since the start of the calculation) to a height of $1.3 \cdot 10^4 km$ from the original position at 1700 km. For $F_M = 10^6$, 10^7, 10^9erg cm^{-2}s^{-1} and the same timespan the corresponding heights are $4300, 7000, 2.7 \cdot 10^4\ km$. This demonstrates that the greater the energy flux, the more violent is the expansion. The explanation for this is found from Fig. 9a, which shows that the highest wave flux creates not only the strongest shocks, but also forms them at the lowest height.

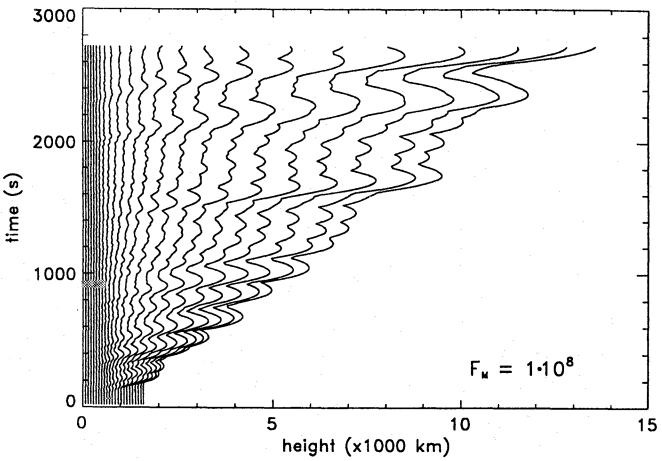

Fig. 10. Time development of the Euler heights of mass elements which were spaced at equal distance in the initial atmosphere

In atmospheres with radiation damping, most of the wave energy is spent to balance the chromospheric radiation loss and very little goes into expansion (see e.g. Cheng 1992). Moreover mechanically heated radiating atmospheres of solar type stars

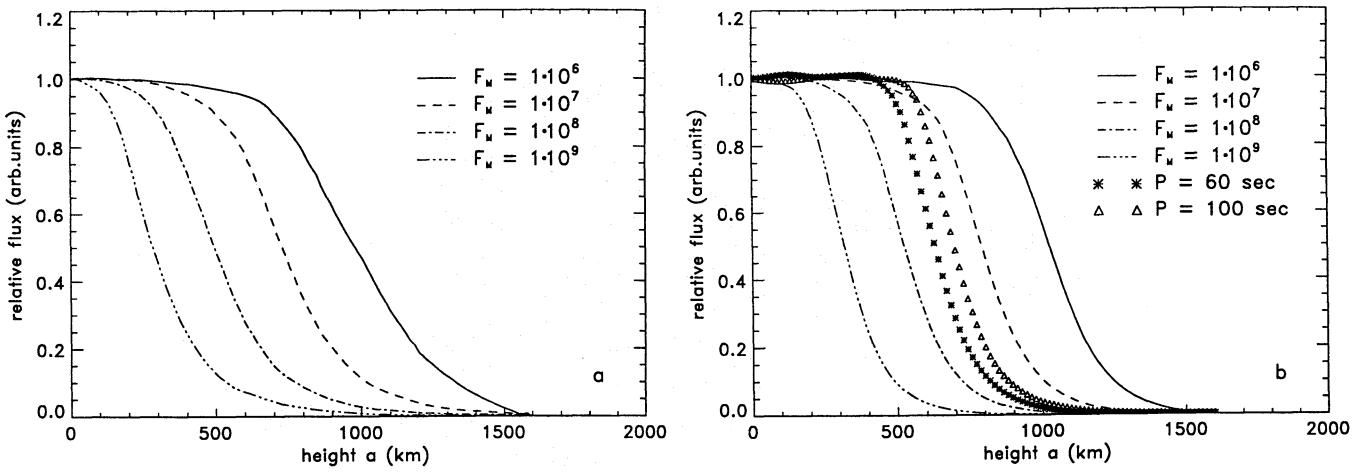

Fig. 11a and b. Mechanical energy fluxes F_M/F_{Mo} as function of height for waves of four different indicated initial fluxes F_{Mo}. **a** For a Gauss spectrum and **b** for monochromatic waves of period P = 35 s. In the latter panel also for monochromatic waves of P = 60 s and P = 100 s with the energy flux $F_M = 1 \cdot 10^8$ erg cm^{-2}s^{-1}

always suffer a "heating catastrophe", that is, a situation where heating overwhelms the cooling and leads to a rapid transition layer temperature rise which limits the extent of the chromospheres (Rammacher & Ulmschneider 1992; Cuntz et al. 1994).

For this reason we have restricted our investigation to Euler heights of less than z_{top} = 2000 km, the observed extent of the solar chromosphere. As seen from Fig. 10 we retain more than 50% of our mass points in that height range which provides sufficient resolution for our purpose. This is particularly so as the shocks are treated with individual height points and the sawtooth shape of the waves can be represented well with a small number of points. However, there is a noticeable flow superposed even over our restricted height slab which may influence our results in an unforseeable way. In subsequent work we therefore intend to repeat the calculations with the inclusion of radiation damping.

3.7. Heating rate as a function of height

Let us finally discuss the dissipation characteristics of our wave calculations and the amount of mechanical energy transmitted through the atmosphere. In Fig. 11a the behaviour of the total acoustic flux as a function of height is shown for a Gauss spectrum with P_{max} = 35 s and four different initial energy fluxes F_M. Very similar dissipation curves versus height, as already discussed in Sect. 3.5 for the average shock strength, are also found for the other spectra. As comparison, Fig. 11b shows the same calculation for a monochromatic wave with period P = 35 s. Here two cases with periods P = 60 and 100 s are also shown. It is seen that the acoustic spectra do not lead to a greatly different dissipation behaviour, although they show a more gradual dissipation. However, the flow discussed in the last section could influence this dissipation characteristic. This question will be addressed in greater detail in a subsequent paper.

For the ratio of the energy flux in the frequency band $<$ 10 mHz emerging at the top of the atmosphere to that entering at the bottom we find the following transmission factors $\mathscr{T} = F_{M,ztop}/F_{M,0}$: 0.5%, 1.1%, 1.2%, 1.7% for $F_M = 1 \cdot 10^6, 1 \cdot 10^7, 1 \cdot 10^8, 1 \cdot 10^9$ erg cm^{-2} s^{-1}, respectively, for the acoustic spectrum, and 0.1%, 0.3% for the monochromatic spectrum with P = 20, 15 s and $F_M = 1 \cdot 10^8$, respectively. The power in the $<$ 10 mHz band constitutes 35% to 60% of the total power and goes up with increasing F_M.

4. Conclusions

From our time-dependent wave calculations in various solar atmosphere models excited by acoustic waves with realistic amplitudes we draw the following conclusions:

1. For excitation with monochromatic waves a critical frequency ν_{cr} is found which separates domains of drastically different resonance behaviour. When excited by waves with frequencies $\nu < \nu_{cr}$ the atmospheric resonance decays rapidly with time, in a similar manner as in the small amplitude wave case of Paper I. For excitation by waves with $\nu > \nu_{cr}$, persistent resonance oscillations are found which are caused by shock overtakings. This case is very similar to an atmosphere excited by a stochastic frequency spectrum discussed in Paper I. Our results are in good general agreement with those of Kalkofen et al. (1994).
2. Excitation by acoustic spectra always leads to the $\nu > \nu_{cr}$ behaviour. Independent of the spectral shape, the wave energy and the atmosphere model, acoustic spectra generate persistent resonance oscillations with frequencies concentrated at ν = 6 – 7 mHz. These results are in good general agreement with those of Fleck & Schmitz (1993) as well as Kalkofen et al. (1994).
3. Adding an evanescent photospheric 5-min oscillation of observed amplitude did not change the resulting power at z = 2000 km height. This is the case both for monochromatic and acoustic wave spectra. 5-min oscillations thus do not play a role in the energy balance of the chromosphere.
4. Shock heating by acoustic spectra is roughly similar to that of a monochromatic wave of period 35 s.

5. Due to the process of shock overtaking, higher initial acoustic fluxes lead to larger fractions of low frequency $\nu < 10$ mHz power.
6. Irrespective of the initial spectral shape and energy and even of the gravity and effective temperature of the star, a universal average shock strength $M_S = 1.5$ is found in our wave calculations. The significance of this is not yet fully understood. It will be discussed in subsequent work.
7. Due to our adiabatic treatment, considerable mass flows and unrealistic extensions of our atmospheric slabs occur. It thus is of great urgency to repeat these calculations with radiation included.

References

Cheng Q.-Q.: 1992, A&A **266**, 549
Cuntz M., Ulmschneider P., Rammacher W.: 1994, ApJ, in press
Deubner F.-L.: 1991, in: *Mechanisms of Chromospheric and Coronal Heating*, Ulmschneider P., Priest E.R., Rosner R., Eds., Springer, Berlin, p. 6
Fleck B., Schmitz F.: 1991, A&A **250**, 235
Fleck B., Schmitz F.: 1993, A&A **273**, 671
Kalkofen W., Rossi P., Bodo G., Massaglia S.: 1994, A&A, **284**, 976
Leibacher J.W., Stein R.F.: 1981, in: *The Sun as a Star*, Jordan S., Ed., NASA SP-450, p. 263
Musielak Z.E., Rosner R., Stein R.F., Ulmschneider P.: 1994, ApJ **423**, 474
Rammacher W., Ulmschneider P.: 1992, A&A **253**, 586
Rutten R.J., Uitenbroek H.: 1991, Solar Phys. **134**, 15
Sutmann G., Ulmschneider P.: 1994, A&A, same issue
Ulmschneider P.: 1989, A&A, 222, 171
Ulmschneider P.: 1990, in: *Cool Stars, Stellar Systems, and the Sun*, Proc. Sixth Cambridge Workshop, G. Wallerstein, Ed., ASP Conf. Series 9, San Francisco, p. 3
Ulmschneider P.: 1991, in: *Mechanisms of Chromospheric and Coronal Heating*, Ulmschneider P., Priest E.R., Rosner R., Eds., Springer, Berlin, p. 328
Ulmschneider P., Rammacher, W., Gail H.-P.: 1992, in: *Cool Stars, Stellar Systems, and the Sun*, Proc. Seventh Cambridge Workshop, M. Giampapa, J. Bookbinder, Eds. ASP Conf. Series 26, San Francisco, p. 471
Vernazza J.E., Avrett E.H., Loeser R.: 1981, ApJS **45**, 635

This article was processed by the author using Springer-Verlag TEX A&A macro package 1992.